

Transport between RGB images motivated by dynamic Optimal Transport

Jan Henrik Fitschen, Friederike Laus and Gabriele Steidl

Department of Mathematics, University of Kaiserslautern, Germany

{fitschen, friederike.laus, steidl}@mathematik.uni-kl.de

March 2, 2022

In this paper we consider the transport between RGB images motivated by the fluid mechanics formulation of the dynamic optimal transport by Benamou and Brenier [7] for $p \in (1, 2]$. Following Papadakis et al. [23] we discretize the problem on a staggered grid in two spatial dimensions, a third dimension for the color and a forth one in time. We propose two different models which relax the continuity equation in dynamic optimal transport. The latter one requires the initial and final image to have the same sum of pixel values, what excludes various color transitions. We show that a minimizer of our discrete models exists, but it is not unique for some special initial/final images. For minimizing the resulting functionals we apply a primal-dual algorithm. Special attention has to be paid to the boundary conditions in the color dimension, where we suggest to use periodic ones. As a consequence, one step of the primal-dual algorithm requires the solution of a four-dimensional Poisson equation with simultaneous zero, mirror and periodic boundary conditions. This can be computed efficiently using fast Sin-I, Cos-II- and Fourier transforms. Numerical examples demonstrate the meaningfulness of our approaches.

1. Introduction

Color image processing is much more challenging compared to gray-value image processing and usually, approaches for gray-value images do not generalize in a straightforward way to color images. For example, one-dimensional histograms are a very simple, but powerful tool in gray-value image processing, while it is in general difficult to exploit histograms of color images. In particular, there exist several possibilities to represent color images [8]. In this paper we consider the interpolation between two color images in the RGB space (see Figure 1 (left)) motivated by the fluid mechanics formulation of dynamic optimal transport by Benamou and Brenier [7] and the recent work of Papadakis

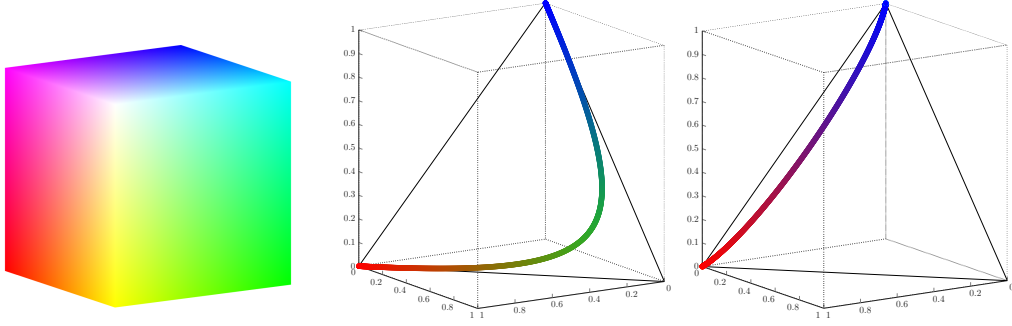


Figure 1: Left: RGB color cube. Middle/Right: Color transfer between $(1,0,0)$ (red) and $(0,0,1)$ (blue) for mirror and periodic boundary conditions visualized in the RGB cube.

et al. [23].

To this end, we interpret the images as three-dimensional density functions f_0 and f_1 of absolutely continuous probability measures $\mu_0 = f_0 dx$ and $\mu_1 = f_1 dx$ in Wasserstein spaces $\mathcal{P}_p(\mathbb{R}^3)$ for $p \in (1, 2]$, where the third dimension is reserved for the color information. In particular, we have $\int_{\mathbb{R}^3} f_0 dx = \int_{\mathbb{R}^3} f_1 dx = 1$, where we assume that the density functions are finitely supported in the two spatial dimensions. Therewith, the intermediate images are obtained as the densities f_t of the geodesic path $\mu_t = f_t dx$ with respect to the Wasserstein distance between μ_0 and μ_1 .

In practical applications, when dealing with discrete images, the continuity equation arising in the fluid mechanics formulation needs to be equipped with spatial boundary conditions. At this point, particular attention has to be paid to the color direction, where we propose to use periodic boundary conditions. This choice is motivated as follows: assume we are given two color pixels f_0 and $f_1 \in \mathbb{R}^{1 \times 1 \times 3}$. Using mirror (Neumann) boundary conditions in the color dimension, the transport of, e.g., a red pixel $f_0 = (1, 0, 0)$ into a blue one $f_1 = (0, 0, 1)$ goes over $(0, 1, 0)$ (green), see Figure 1 (middle), which is not intuitive from the viewpoint of human color perception. Furthermore, it implies that the transport depends on the order of the three color channels, which is clearly not desirable. As a remedy, we suggest to use periodic boundary conditions in the color dimension. In case of a red and a blue pixel, it yields a transport via violet, which is also what one would expect, compare Figure 1 (right) and see also Figure 4.

The interpretation of a color image as a probability density function has a major drawback: To represent a valid density, the sums of all pixel values of the given images have to be one (or at least equal). While rescaling might be an option for color images with nearly the same mass, the results are usually not realistic for arbitrary color images. In our motivating example this means that we can only transport colors that lie in the intersection of the hyperplane $\{x \in \mathbb{R}^3 : x_1 + x_2 + x_3 = 1\}$ with the RGB cube. As a consequence, it is for instance not possible to transport a red pixel $f_0 = (1, 0, 0)$ into a yellow one $f_1 = (1, 1, 0)$. Rescaling would yield a transport into $(\frac{1}{2}, \frac{1}{2}, 0)$ which is not satisfying. Therefore we propose two models where the mass conservation constraint is relaxed. It turns out that a relaxed version of our model is just a reinterpretation of

the model that was proposed in [23] for gray-value images. A second model penalizes the continuity constraint as it was also considered in a continuous framework by Maas et al. [22].

Extensive work on image interpolation has been done by Peyré and co-workers, besides [23] we refer e.g. to [25, 29]. For the transfer between color images, in particular with respect the HSV color model and measures on the circle, we point to the papers of Delon et al. [18, 28]. Finally we mention that the interpolation between images can also be tackled by other techniques such as metamorphoses, see [34]. A combination of the optimal dynamic transport model with the metamorphosis approach was proposed in [22].

The outline of our paper is as follows: in Section 2 we recall basic results from the theory of optimal transport, before we propose discrete transport models in Section 3. We prefer to give a matrix-vector notation of the problem to make it more intuitive from the linear algebra point of view. We prove the existence of a minimizer and show that there are special settings where the minimizer is not unique. In Section 4 we solve the resulting minimization problems by primal-dual minimization algorithms. It turns out that one step of the algorithm requires the solution of a four-dimensional Poisson equation which includes zero, mirror and periodic boundary conditions and can be handled by fast trigonometric transforms. Another step involves to find the positive root of a polynomial of degree $2q - 1$, where $\frac{1}{p} + \frac{1}{q} = 1$. For this task we propose to use Newton's algorithm and determine an appropriate starting point to ensure its quadratic convergence. Section 5 shows numerical results, some of which were also reported at the SampTA conference 2015 [19]. Finally, Section 6 contains conclusions. The Appendix reviews the diagonalization of certain discrete Laplace operators, and provides basic rules for tensor product computations.

2. Dynamic Optimal Transport

In this section we briefly review some basic facts on the theory of optimal transport, for further details we refer to, e.g. [1, 35].

Let $\mathcal{P}(\mathbb{R}^d)$ be the space of probability measures on \mathbb{R}^d and $\mathcal{P}_p(\mathbb{R}^d)$, $p \in [1, \infty)$ the Wasserstein space of measures having finite p -th moments

$$\mathcal{P}_p(\mathbb{R}^d) := \left\{ \mu \in \mathcal{P}(\mathbb{R}^d) : \int_{\mathbb{R}^d} |x|^p d\mu(x) < +\infty \right\}.$$

For $\mu_0, \mu_1 \in \mathcal{P}(\mathbb{R}^d)$ let $\Pi(\mu_0, \mu_1)$ be the set of all probability measures on $\mathbb{R}^d \times \mathbb{R}^d$ whose marginals are equal to μ_0 and μ_1 . Therewith, the optimal transport problem (Kantorovich problem) reads as

$$\operatorname{argmin}_{\gamma \in \Pi(\mu_0, \mu_1)} \int_{\mathbb{R}^d} |x - y|^p d\gamma(x, y).$$

One can show that for $p \in [1, \infty)$ a minimizer exists, which is uniquely determined for $p > 1$ and also called optimal transport plan. In the special case of the one-dimensional

optimal transport problem, if the measure μ_0 is non-atomic, the optimal transport plan is the same for all $p \in (1, \infty)$ and can be stated explicitly in terms of the cumulative density functions of the involved measures. The minimal value

$$W_p(\mu_0, \mu_1) := \min_{\gamma \in \Pi(\mu_0, \mu_1)} \int_{\mathbb{R}^d} |x - y|^p d\gamma(x, y)$$

defines a distance on $\mathcal{P}_p(\mathbb{R}^d)$, the so-called *Wasserstein distance*.

Wasserstein spaces $(\mathcal{P}_p(\mathbb{R}^d), W_p(\mathbb{R}^d))$ are geodesic spaces. In particular, there exists for any $\mu_0, \mu_1 \in \mathcal{P}_p(\mathbb{R}^d)$ a geodesic $\gamma: [0, 1] \rightarrow \mathcal{P}_p(\mathbb{R}^d)$ with $\gamma(0) = \mu_0$ and $\gamma(1) = \mu_1$. For interpolating our images we ask for $\mu_t = \gamma(t)$, $t \in [0, 1]$.

At least theoretically there are several ways to compute μ_t . If the optimal transport plan γ is known, then $\mu_t = \mathcal{L}_{t\#}\gamma := \gamma \circ \mathcal{L}_t^{-1}$ yields the geodesic path, where $\mathcal{L}_t: \mathbb{R}^d \times \mathbb{R}^d \rightarrow \mathbb{R}^d$ is the linear interpolation map $\mathcal{L}_t(x, y) = (1 - t)x + ty$. This requires the knowledge of the optimal transport plan γ and of \mathcal{L}_t^{-1} . At the moment there are efficient ways for computing the optimal transport plan γ only in special cases, in particular in the one-dimensional case by an ordering procedure and for Gaussian distributions in the case $p = 2$ using expectation and covariance matrix. For $p = 2$ one can also use the fact that γ is indeed induced by a transport map $T: \mathbb{R}^d \rightarrow \mathbb{R}^d$, i.e., $\gamma = (\text{id}, T)_\# \mu_0$, which can be written as $T = \nabla \psi$, where ψ fulfills the Monge-Ampère equation, see [10]. However, this second order nonlinear elliptic PDE is numerically hard to solve and so far, only some special cases were considered [6, 12, 13, 21]. Other numerical techniques to compute optimal transport plans have been proposed, e.g., in [2, 20, 32]. Another approach consists in relaxing the condition of minimizing a Wasserstein distance by using instead an entropy regularized Wasserstein distance. Such distances can be computed more efficiently by the Sinkhorn algorithm and were applied within a barycentric approach by Cuturi et al. [14, 15].

In this paper we focus on the approach of Benamou and Brenier in [7] which involves the speed of geodesic curves joining μ_0 and μ_1 . If $v: \mathbb{R}_{\geq 0} \times \mathbb{R}^d \rightarrow \mathbb{R}^d$ is any velocity field whose flow captures the spatial evolution from the distribution μ_0 to μ_1 , then it can be shown that the energy functional

$$\mathcal{E}_p(\mu, v) := \int_0^1 \int_{\mathbb{R}^d} \frac{1}{p} |v(x, t)|^p d\mu_t(x) dt \quad (1)$$

fulfills $\mathcal{E}_p(\mu, v) \geq \frac{1}{p} W_p^p(\mu_0, \mu_1)$. Further, if γ is an optimal transport plan between μ_0 and μ_1 and $\mu_t = \mathcal{L}_{t\#}\gamma$, then it holds that for every $y \in \text{supp}(\mu_t)$ there exists a unique pair $(X_t(y), Z_t(y)) \in \text{supp}(\gamma)$ with $y = (1 - t)X_t(y) + tZ_t(y)$, so that the velocity field $v(t, \cdot) := Z_t - X_t$, $t \in (0, 1)$ is well defined on $\text{supp}(\mu_t)$ and satisfies

$$\|v(t, \cdot)\|_{L^p(\mu_t)} = W_p(\mu_0, \mu_1).$$

This means, the velocity field $v(t, \cdot)$ has constant speed and minimizes the energy functional (1). Further, the continuity equation

$$\begin{aligned} \partial_t \mu_t + \nabla_x \cdot (\mu_t v(t, \cdot)) &= 0, \\ \|v(t, \cdot)\|_{L^p(\mu_t)} &= W_p(\mu_0, \mu_1), \end{aligned}$$

is fulfilled, where we say that $t \mapsto \mu_t$ is a measure-valued solution of the continuity equation if for all $\phi \in C_c^1((0, 1) \times \mathbb{R}^d)$ and $T \in (0, 1)$ the relation

$$\int_0^T \int_{\mathbb{R}^d} \partial_t \phi(x, t) + \langle v(x, t), \nabla_x \phi(x, t) \rangle d\mu_t(x) dt = 0$$

holds true. Assuming the measures μ_0 and μ_1 to be absolutely continuous with respect to the Lebesgue measure, i.e. $\mu_0 = f_0 dx$ and $\mu_1 = f_1 dx$, theoretical results (see for instance [35, Theorem 8.7]) guarantee that the same holds true for $\mu_t = f_t dx$, where f_t can be obtained as the minimizer over v, f of

$$\mathcal{E}_p(v, f) = \int_0^1 \int_{\mathbb{R}^d} \frac{1}{p} |v(x, t)|^p f(x, t) dx dt \quad (2)$$

subject to the continuity equation

$$\begin{aligned} \partial_t f(x, t) + \nabla_x \cdot (v(x, t) f(x, t)) &= 0, \\ f(0, \cdot) &= f_0, \quad f(1, \cdot) = f_1, \end{aligned}$$

where we suppose $\cup_{t \in [0, 1]} \text{supp } f(t, \cdot) \subseteq [0, 1]^d$ with appropriate (spatial) boundary conditions. Unfortunately, the energy functional (2) is not convex in f and v . Therefore, Benamou and Brenier suggested a change of variables $(f, v) \mapsto (f, fv) = (f, m)$. For $p \in (1, \infty)$ this results in the functional

$$\int_0^1 \int_{\mathbb{R}^d} J_p(m(x, t), f(x, t)) dx dt, \quad (3)$$

where $J_p: \mathbb{R}^d \times \mathbb{R} \rightarrow \mathbb{R} \cup \{+\infty\}$ is defined as

$$J_p(x, y) := \begin{cases} \frac{1}{p} \frac{|x|^p}{y^{p-1}} & \text{if } y > 0, \\ 0 & \text{if } (x, y) = (0, 0), \\ +\infty & \text{otherwise} \end{cases} \quad (4)$$

and $|\cdot|$ denotes the Euclidean norm. This functional has to be minimized subject to the continuity equation

$$\partial_t f(x, t) + \nabla_x \cdot m(x, t) = 0, \quad (5)$$

$$f(0, \cdot) = f_0, \quad f(1, \cdot) = f_1, \quad (6)$$

equipped with appropriate spatial boundary conditions.

Remark 1. The function $J_p: \mathbb{R}^d \times \mathbb{R} \rightarrow \mathbb{R} \cup \{+\infty\}$ defined in (4) is the perspective function of $\psi(s) = \frac{1}{p} |s|^p$, i.e., $J_p(x, y) = y \psi\left(\frac{x}{y}\right)$. For properties of perspective functions see, e.g., [16]. In particular, since ψ is convex for $p \in (1, \infty)$, its perspective $J_p(x, y)$ is also convex. Further, $J_p(x, y)$ is lower semi-continuous and positively homogeneous, i.e. $J_p(\lambda x, \lambda y) = \lambda J_p(x, y)$ for all $\lambda > 0$.

3. Discrete Transport Models

In practice we are dealing with discrete images whose pixel values are given on a rectangular grid. To get a discrete version of the minimization problem we have to discretize both the integration operator in (3) by a quadrature rule and the differential operators in the continuity equation (5). The discretization of the continuity equation requires the evaluation of discrete “partial derivatives” in time as well as in space. In order to avoid solutions suffering from the well known checkerboard-effect (see for instance [24]) we adopt the idea of a staggered grid as in [23], see Figure 2.

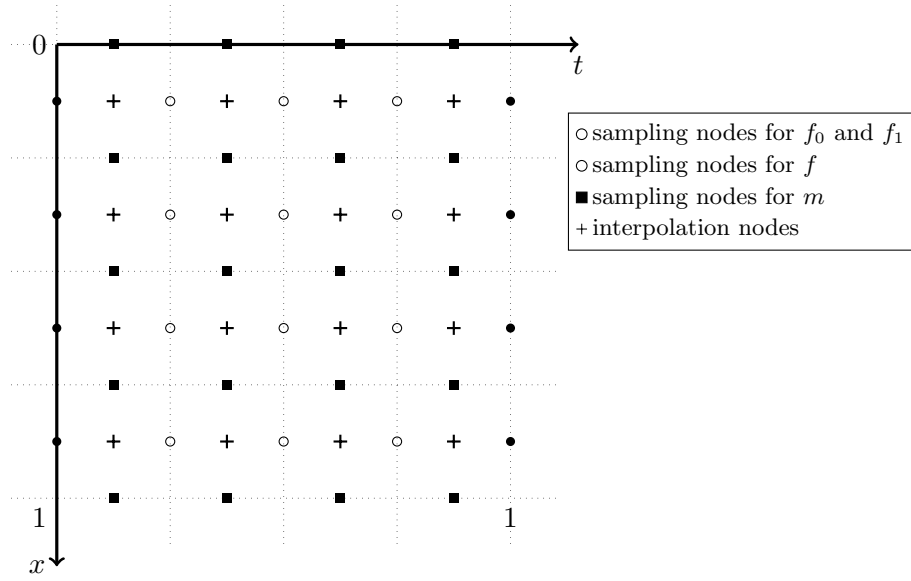


Figure 2: Staggered grid for the discretization of the dynamic optimal transport problem, where $N = P = 4$.

The differential operators are discretized by forward differences, and depending on the boundary conditions this results in the use of difference matrices of the form

$$D_n := n \begin{pmatrix} -1 & 1 & & & & \\ & -1 & 1 & & & \\ & & & \ddots & & \\ & & & & -1 & 1 & 0 \\ & & & & & -1 & 1 \end{pmatrix} \in \mathbb{R}^{n-1,n}, \quad D_n^{\text{per}} := n \begin{pmatrix} 1 & & & & -1 \\ -1 & 1 & & & \\ & & \ddots & & \\ & & & 1 & 0 \\ & & & -1 & 1 \end{pmatrix} \in \mathbb{R}^{n,n}.$$

For the integration we apply a simple midpoint rule. To handle this part, we introduce the averaging/interpolation matrices

$$S_n := \frac{1}{2} \begin{pmatrix} 1 & & & & & \\ & 1 & & & & \\ & & 1 & & & \\ & & & 1 & & \\ & & & & \ddots & \\ & & & & & 1 & 1 \end{pmatrix} \in \mathbb{R}^{n-1,n}, \quad S_n^{\text{per}} := \frac{1}{2} \begin{pmatrix} 1 & 0 & & & & 1 \\ 1 & 1 & & & & \\ & 1 & 1 & & & \\ & & & \ddots & & \\ & & & & 1 & 1 & 0 \\ & & & & & 1 & 1 \end{pmatrix} \in \mathbb{R}^{n,n}.$$

Discretization for one spatial dimension + time: In the following, we derive the discretization of (3) for one spatial direction, i.e., for the transport of signals. The problem can be formulated in a simple matrix-vector form using tensor products of matrices which makes it rather intuitive from the linear algebra point of view. Moreover, it will be helpful for deriving the fast trigonometric transforms which will play a role within our algorithm. We generalize the approach to higher dimensions at the end of this section.

We want to organize the transport between two given one-dimensional, nonnegative discrete signals

$$f_0 := \left(f_0(\frac{j-1/2}{N}) \right)_{j=1}^N \quad \text{and} \quad f_1 := \left(f_1(\frac{j-1/2}{N}) \right)_{j=1}^N.$$

We are looking for the intermediate signals f_t for $t = \frac{k}{P}$, $k = 1, \dots, P-1$. Using the notation $f_t(x) = f(x, t)$, we want to find $f(\frac{j-1/2}{N}, \frac{k}{P})_{j=1, k=1}^{N, P-1} \in \mathbb{R}^{N, P-1}$. For m we have to take the boundary conditions into account. The values of m are taken at the cell faces $\frac{j}{N}$, $j = \kappa, \dots, N-1$ and time $\frac{k-1/2}{P}$, $k = 1, \dots, P$, i.e., we are looking for $\left(m(\frac{j}{N}, \frac{k-1/2}{P}) \right)_{j=\kappa, k=1}^{N-1, P} \in \mathbb{R}^{N-\kappa, P}$, where

$$\kappa = \begin{cases} 1 & \text{mirror boundary,} \\ 0 & \text{periodic boundary.} \end{cases}$$

The midpoints for the quadrature rule are computed by averaging the neighboring two values of m and f , respectively. To give a sound matrix-vector notation of the discrete minimization problem we reorder m and f columnwise into vectors $\text{vec}(f) \in \mathbb{R}^{N(P-1)}$ and $\text{vec}(m) \in \mathbb{R}^{(N-\kappa)P}$, which we again denote by f and m . For the vec operator in connection with the tensor product \otimes of matrices we refer to Appendix B. More specifically, let

$$\begin{aligned} S_f &:= S_P^T \otimes I_N, & D_f &:= D_P^T \otimes I_N, \\ S_m &:= \begin{cases} I_P \otimes S_N^T & \text{mirror boundary,} \\ I_P \otimes (S_N^{\text{per}})^T & \text{periodic boundary,} \end{cases} \\ D_m &:= \begin{cases} I_P \otimes D_N^T & \text{mirror boundary,} \\ I_P \otimes (D_N^{\text{per}})^T & \text{periodic boundary.} \end{cases} \end{aligned}$$

Finally, we introduce the vectors

$$\begin{aligned} f^+ &:= \frac{1}{2}(f_0^T, \mathbf{0}, f_1^T)^T, \\ f^- &:= P(-f_0^T, \mathbf{0}, f_1^T)^T, \end{aligned}$$

where we denote by $\mathbf{0}$ (and $\mathbf{1}$) arrays of appropriate size with entries 0 (and 1). Now the continuity equation (5) together with the boundary conditions (6) for f can be reformulated as requirement that (m, f) has to lie within the hyperplane

$$\mathcal{C}_0 := \left\{ \begin{pmatrix} m \\ f \end{pmatrix} : \underbrace{(D_m | D_f)}_A \begin{pmatrix} m \\ f \end{pmatrix} = f^- \right\}. \quad (7)$$

We will see in Proposition 5 that AA^T is rank one deficient. Since further $\mathbf{1}^T A = \mathbf{0}$, we conclude that the under-determined linear system in (7) has a solution if and only if $\mathbf{1}^T f^- = 0$, i.e., if and only if f_0 and f_1 have the same mass

$$\mathbf{1}^T f_0 = \mathbf{1}^T f_1. \quad (8)$$

This resembles the fact that dynamic optimal transport is performed between probability measures. However, in this paper we consider more general the set

$$\mathcal{C} := \operatorname{argmin}_{(m, f)} \|(D_m | D_f) \begin{pmatrix} m \\ f \end{pmatrix} - f^-\|_2^2.$$

Note that the boundary conditions (6) for f are preserved, while the mass conservation (8) is no longer required. Clearly, if (8) holds true, then \mathcal{C} coincides with \mathcal{C}_0 . Let $\iota_{\mathcal{C}}$ denote the indicator function of \mathcal{C} defined by

$$\iota_{\mathcal{C}}(x) := \begin{cases} 0 & \text{if } x \in \mathcal{C}, \\ +\infty & \text{if } x \notin \mathcal{C}. \end{cases}$$

For $p \in (1, 2]$, we consider the following transport problem:

Constrained Transport Problem:

$$\operatorname{argmin}_{(m, f)} E(m, f) := \|J_p(S_m m, S_f f + f^+)\|_1 + \iota_{\mathcal{C}}(m, f). \quad (9)$$

Here, the application of J_p is meant componentwise and the summation over its (non-negative) components is addressed by the ℓ_1 -norm. The interpolation operators S_m and S_f arise from the midpoint rule for computing the integral.

We can further relax the relaxed continuity assumption $(m, f) \in \mathcal{C}$ by replacing it by

$$\|(D_m | D_f) \begin{pmatrix} m \\ f \end{pmatrix} - f^-\|_2^2 \leq \tau,$$

where $\tau \geq \tau_0 := \min_{(m, f)} \|(D_m | D_f)(m^T, f^T)^T - f^-\|_2^2$. For $\tau = \tau_0$ we have again problem (9). Since there is a correspondence between the solutions of such constrained problems

with parameter τ and the penalized problem with a corresponding parameter λ , see [3, 30, 33], we prefer to consider the following penalized problem with regularization parameter $\lambda > 0$:

Penalized Transport Problem:

$$\operatorname{argmin}_{(m,f)} E_\lambda(m, f) := \|J_p(S_m m, S_f f + f^+)\|_1 + \lambda \|(D_m | D_f) \begin{pmatrix} m \\ f \end{pmatrix} - f^-\|_2^2. \quad (10)$$

Note that also for our penalized model the boundary conditions (6) for f still hold true. For the continuous setting a penalized model was examined in [22].

To show the existence of a solution of the discrete transport problems we use the concept of asymptotically level stable functions. As usual, for a function $F: \mathbb{R}^n \rightarrow \mathbb{R} \cup \{+\infty\}$ and $\mu > \inf_x E(x)$, the level sets are defined by

$$\operatorname{lev}(F, \mu) := \{x \in \mathbb{R}^n : F(x) \leq \mu\}.$$

By F_∞ we denote the *asymptotic (or recession) function* of F which according to [17], see also [4, Theorem 2.5.1], can be computed by

$$F_\infty(x) = \liminf_{\substack{x' \rightarrow x \\ t \rightarrow \infty}} \frac{F(tx')}{t}.$$

The following definition of *asymptotically level stable* functions is taken from [4, p. 94]: a proper and lower semicontinuous function $F: \mathbb{R}^n \rightarrow \mathbb{R} \cup \{+\infty\}$ is said to be *asymptotically level stable* if for each $\rho > 0$, each real-valued, bounded sequence $\{\mu_k\}_k$ and each sequence $\{x_k\}_k$ satisfying

$$x_k \in \operatorname{lev}(F, \mu_k), \quad \|x_k\|_2 \rightarrow +\infty, \quad \frac{x_k}{\|x_k\|_2} \rightarrow \tilde{x} \in \ker(F_\infty), \quad (11)$$

there exists k_0 such that

$$x_k - \rho \tilde{x} \in \operatorname{lev}(F, \mu_k) \quad \text{for all } k \geq k_0.$$

If for each real-valued, bounded sequence $\{\mu_k\}_k$ there exists no sequence $\{x_k\}_k$ satisfying (11), then F is automatically asymptotically level stable. In particular, coercive functions are asymptotically level stable. It was originally exhibited in [5] (without the notion of asymptotically level stable functions) that any asymptotically level stable function F with $\inf F > -\infty$ has a global minimizer. A proof was also given in [4, Corollary 3.4.2]. With these preliminaries we can prove the existence of minimizers of our transport models.

Proposition 2. *The discretized dynamic transport models (9) and (10) have a solution.*

Proof. We show that the proper, lower semicontinuous functions E and E_λ are asymptotically level stable which implies the existence of a minimizer. For the penalized problem, the asymptotic function $E_{\lambda,\infty}$ reads

$$E_{\lambda,\infty}(m, f) = \liminf_{\substack{(m', f') \rightarrow (m, f), \\ t \rightarrow \infty}} \frac{E_\lambda(t(m', f'))}{t}.$$

We obtain

$$\begin{aligned} \frac{E_\lambda(t(m', f'))}{t} &= \frac{1}{t} \left(\|J_p(t(S_m m', S_f f' + f^+))\|_1 + \lambda \|(D_m | D_f) \begin{pmatrix} t m' \\ t f' \end{pmatrix} - f^-\|_2^2 \right) \\ &= \|J_p(S_m m', S_f f' + \frac{1}{t} f^+)\|_1 + \lambda t \|(D_m | D_f) \begin{pmatrix} m' \\ f' \end{pmatrix} - \frac{1}{t} f^-\|_2^2. \end{aligned}$$

Thus, $(\tilde{m}, \tilde{f}) \in \ker(E_{\lambda,\infty})$ implies

$$(\tilde{m}, \tilde{f}) \in \ker(D_m | D_f), \quad \tilde{m} \in \ker(S_m), \quad S_f \tilde{f} \geq 0. \quad (12)$$

For the constrained problem we have the same implications so that we can restrict our attention to the penalized one. By the definition of S_m we obtain

$$\ker(S_m) = \begin{cases} \{w \otimes \tilde{\mathbf{1}} : w \in \mathbb{R}^P\} & \text{for periodic boundary conditions and even } N, \\ \{\mathbf{0}\} & \text{otherwise,} \end{cases}$$

where $\tilde{\mathbf{1}} = (1, -1, \dots, 1, -1)^T \in \mathbb{R}^N$. In the case $\ker(S_m) = \{\mathbf{0}\}$, the first and second condition in (12) imply $D_f \tilde{f} = 0$ so that by the definition of D_f also $\tilde{f} = 0$. In the other case, we obtain by the first condition in (12) that $\tilde{f} = D_f^\dagger D_m \tilde{m}$, where $D_f^\dagger = (D_f^T D_f)^{-1} D_f^T$ denotes the Moore-Penrose inverse of D_f . Then

$$S_f \tilde{f} = S_f D_f^\dagger D_m \tilde{m} = S_f D_f^\dagger D_m (w \otimes \tilde{\mathbf{1}})$$

for some $w \in \mathbb{R}^P$. Straightforward computation shows

$$S_f \tilde{f} = S_f D_f^\dagger D_m (w \otimes \tilde{\mathbf{1}}_N) = \tilde{w} \otimes \tilde{\mathbf{1}}_N$$

for some $\tilde{w} \in \mathbb{R}^P$. Now the third condition in (12) can only be fulfilled if $\tilde{w} = \mathbf{0}$. Consequently we have in both cases

$$S_f \tilde{f} = 0. \quad (13)$$

Let $\rho > 0$, $\{\mu_k\}_k$ be a bounded sequence and $\{(m_k, f_k)\}_k$ be a sequence fulfilling (11). By (12) and (13) we conclude

$$\begin{aligned} E_\lambda((m_k, f_k) - \rho(\tilde{m}, \tilde{f})) &= \|J_p(S_m m_k, S_f f_k + f^+)\|_1 + \lambda \|(D_m | D_f) \begin{pmatrix} m_k \\ f_k \end{pmatrix} - f^-\|_2^2 \\ &= E_\lambda((m_k, f_k)). \end{aligned}$$

Since $(m_k, f_k) \in \text{lev}(E_\lambda, \mu_k)$, this shows that $(m_k, f_k) - \rho(\tilde{m}, \tilde{f}) \in \text{lev}(E_\lambda, \lambda_k)$ as well and finishes the proof. \square

Unfortunately, $J_p(u, v)$ is not strictly convex on its domain as it can be deduced from the following proposition.

Proposition 3. *For any two minimizers (m_i, f_i) , $i = 1, 2$ of (9) the relation*

$$\frac{S_m m_1}{S_f f_1 + f^-} = \frac{S_m m_2}{S_f f_2 + f^-}$$

holds true.

Proof. We use the perspective function notation from Remark 1. For $\lambda \in (0, 1)$ and (u_i, v_i) with $v_i > 0$, $i = 1, 2$, we have (componentwise)

$$\begin{aligned} J_p(\lambda(u_1, v_1) + (1 - \lambda)(u_2, v_2)) &= (\lambda v_1 + (1 - \lambda)v_2) \psi \left(\frac{\lambda u_1 + (1 - \lambda)u_2}{\lambda v_1 + (1 - \lambda)v_2} \right) \\ &= (\lambda v_1 + (1 - \lambda)v_2) \psi \left(\frac{\lambda v_1}{\lambda v_1 + (1 - \lambda)v_2} \frac{u_1}{v_1} + \frac{(1 - \lambda)v_2}{\lambda v_1 + (1 - \lambda)v_2} \frac{u_2}{v_2} \right) \end{aligned}$$

and if $\frac{u_1}{v_1} \neq \frac{u_2}{v_2}$ by the strict convexity of ψ that

$$J_p(\lambda(u_1, v_1) + (1 - \lambda)(u_2, v_2)) < \lambda J_p(u_1, v_1) + (1 - \lambda) J_p(u_2, v_2).$$

Setting $u_i := S_m m_i$ and $v_i := S_f f_i + f^-$, $i = 1, 2$, we obtain the assertion. \square

Remark 4. *For periodic boundary conditions, even N and $f_1 = f_0 + \gamma \tilde{\mathbf{1}}$, $\gamma \in [0, \min f_0]$ the minimizer of (9) is not unique. This can be seen as follows: Obviously, we would have a minimizer (m, f) if $m = w \otimes \tilde{\mathbf{1}} \in \ker(S_m)$ for some $w \in \mathbb{R}^P$ and there exists $f \geq 0$ which fulfills the constraints. Setting $f^{k/P} := f(j - 1/2, k)_{j=1}^N$, $k = 0, \dots, P$, these constraints read $-2Pw \otimes \tilde{\mathbf{1}} = P(f^{(k-1)/P} - f^{k/P})_{k=1}^P$. Thus, any $w \in \mathbb{R}^P$ such that*

$$\begin{aligned} f^{1/P} &= f_0 + 2w_1 \tilde{\mathbf{1}}, \quad f^{2/P} = f_0 + 2(w_1 + w_2) \tilde{\mathbf{1}}, \dots, \\ f^1 &= f_0 + 2(w_1 + w_2 + \dots + w_P) \tilde{\mathbf{1}} \end{aligned}$$

are nonnegative vectors provides a minimizer of (9). We conjecture that the solution is unique in all other cases, but have no proof so far.

Discretization for three spatial dimensions + time: For RGB images of size $N_1 \times N_2 \times N_3$, where $N_3 = 3$, we have to work in three spatial dimensions. Setting $N := (N_1, N_2, N_3)$, $j := (j_1, j_2, j_3)$ and defining the quotient $\frac{j}{N}$ componentwise we obtain

- $f_i = \left(f_i \left(\frac{j-1/2}{N} \right) \right)_{j=(1,1,1)}^N \in \mathbb{R}^{N_1, N_2, N_3}$, $i = 0, 1$,
- $f = \left(f \left(\frac{j-1/2}{N}, \frac{k}{P} \right) \right)_{j=(1,1,1), k=1}^{N, P-1} \in \mathbb{R}^{N_1, N_2, 3, P-1}$,

- $m = (m_1, m_2, m_3)$, with

$$\begin{aligned} & \left(m_1 \left(\frac{j_1}{N_1}, \frac{j_2-1/2}{N_2}, \frac{j_3-1/2}{3}, \frac{k-1/2}{P} \right) \right)_{j_1=1, j_2=1, j_3=1, k=1}^{N_1-1, N_2, 3, P} \in \mathbb{R}^{N_1-1, N_2, 3, P}, \\ & \left(m_2 \left(\frac{j_1-1/2}{N_1}, \frac{j_2}{N_2}, \frac{j_3-1/2}{3}, \frac{k-1/2}{P} \right) \right)_{j_1=1, j_2=1, j_3=1, k=1}^{N_1, N_2-1, 3, P} \in \mathbb{R}^{N_1, N_2-1, 3, P}, \\ & \left(m_3 \left(\frac{j_1-1/2}{N_1}, \frac{j_2-1/2}{N_2}, \frac{j_3}{3}, \frac{k-1/2}{P} \right) \right)_{j_1=1, j_2=1, j_3=0, k=1}^{N_1, N_2, 2, P} \in \mathbb{R}^{N_1, N_2, 3, P}. \end{aligned}$$

In the definition of m we take the periodic boundary for the third spatial direction into account. Analogously as in the one-dimensional case, when reshaping m and f into long vectors, the interpolation and differentiation operators can be written using tensor products. For the interpolation operator we have

$$S_m m = \begin{pmatrix} (I_P \otimes I_3 \otimes I_{N_2} \otimes S_{N_1}^T) m_1 \\ (I_P \otimes I_3 \otimes S_{N_2}^T \otimes I_{N_1}) m_2 \\ (I_P \otimes S_3^T \otimes I_{N_2} \otimes I_{N_1}) m_3 \end{pmatrix} \quad \text{and} \quad S_f f = (S_P^T \otimes I_3 \otimes I_{N_2} \otimes I_{N_1}) f,$$

which means, that $S_m m$ computes the average of m_i with respect to the i -th coordinate, $i = 1, 2, 3$, and $S_f f$ computes the average of f with respect to the time variable. Similarly we generalize the differentiation operator, see (17). In this sense we will use the same notation as in the previous paragraph and consider just linear operators.

4. Primal-Dual Minimization Algorithm

4.1. Algorithms

For the minimization of our functionals we apply the primal-dual algorithm known as Chambolle-Pock algorithm [11, 26] in the form of Algorithm 8 in [9]. We use the following reformulation of the problems:

Constrained Transport Problem:

$$\begin{aligned} & \underset{(m, f)}{\operatorname{argmin}} \|J_p(u, v)\|_1 + \iota_C(m, f) \\ & \text{subject to } S_m m = u, S_f f + f^+ = v. \end{aligned} \tag{14}$$

Penalized Transport Problem:

$$\begin{aligned} & \underset{(m, f)}{\operatorname{argmin}} \|J_p(u, v)\|_1 + \lambda \left\| \underbrace{(D_m | D_f)}_A \begin{pmatrix} m \\ f \end{pmatrix} - f^- \right\|_2^2 \\ & \text{subject to } S_m m = u, S_f f + f^+ = v. \end{aligned} \tag{15}$$

In the following we detail the first two steps of Algorithms 1 and 2:

Algorithm 1: Primal-Dual Algorithm for the Constrained Problem (14)

Initialization: $m^{(0)} = \mathbf{0}$, $f^{(0)} = \mathbf{0}$, $b_m^{(0)} = b_f^{(0)} = \bar{b}_u^{(0)} = \bar{b}_v^{(0)} = \mathbf{0}$, $\theta \in (0, 1]$,
 τ, σ with $\tau\sigma < 1$.

Iteration: For $r = 0, 1, \dots$ iterate

1. $\begin{pmatrix} m^{(r+1)} \\ f^{(r+1)} \end{pmatrix} := \operatorname{argmin}_{(m,f) \in \mathcal{C}} \frac{1}{2\tau} \left\| \begin{pmatrix} m \\ f \end{pmatrix} - \begin{pmatrix} m^{(r)} \\ f^{(r)} \end{pmatrix} + \tau\sigma \begin{pmatrix} S_m^T \bar{b}_u^{(r)} \\ S_f^T \bar{b}_v^{(r)} \end{pmatrix} \right\|_2^2$
 2. $\begin{pmatrix} u^{(r+1)} \\ v^{(r+1)} \end{pmatrix} := \operatorname{argmin}_{(u,v)} J_p(u, v) + \frac{\sigma}{2} \left\| \begin{pmatrix} u \\ v \end{pmatrix} - \begin{pmatrix} S_m m^{(r+1)} \\ S_f f^{(r+1)} \end{pmatrix} - \begin{pmatrix} 0 \\ f_b^+ \end{pmatrix} - \begin{pmatrix} b_u^{(r)} \\ b_v^{(r)} \end{pmatrix} \right\|_2^2$
 3. $b_u^{(r+1)} := b_u^{(r)} + S_m m^{(r+1)} - u^{(r+1)}$
 $b_v^{(r+1)} := b_v^{(r)} + S_f f^{(r+1)} + f_b^+ - v^{(r+1)}$
 4. $\bar{b}_u^{(r+1)} := b_u^{(r+1)} + \theta(b_u^{(r+1)} - b_u^{(r)})$
 $\bar{b}_v^{(r+1)} := b_v^{(r+1)} + \theta(b_v^{(r+1)} - b_v^{(r)})$
-

Algorithm 2: Primal-Dual Algorithm for the Penalized Problem (15)

Initialization: $m^{(0)} = \mathbf{0}$, $f^{(0)} = \mathbf{0}$, $b_u^{(0)} = b_v^{(0)} = \bar{b}_u^{(0)} = \bar{b}_v^{(0)} = \mathbf{0}$, $\theta \in (0, 1]$,
 τ, σ with $\tau\sigma < 1$.

Iteration: For $r = 0, 1, \dots$ iterate

1. $\begin{pmatrix} m^{(r+1)} \\ f^{(r+1)} \end{pmatrix} := \operatorname{argmin}_{(m,f)} \frac{\lambda}{2} \|(D_m | D_f) \begin{pmatrix} m \\ f \end{pmatrix} - f_b^-\|_2^2$
 $+ \frac{1}{2\tau} \left\| \begin{pmatrix} m \\ f \end{pmatrix} - \begin{pmatrix} m^{(r)} \\ f^{(r)} \end{pmatrix} + \tau\sigma \begin{pmatrix} S_m^T \bar{b}_u^{(r)} \\ S_f^T \bar{b}_v^{(r)} \end{pmatrix} \right\|_2^2$
 - 2 – 5. as in Algorithm 1
-

- Step 1 of Algorithm 1 requires the projection onto \mathcal{C} ,
- Step 1 of Algorithm 2 results in the solution of a linear system of equations with coefficient matrix $\lambda A^T A + \frac{1}{\tau} I$ whose Schur complement can be computed via fast trigonometric transforms,
- Step 2 of both algorithms is the proximal map of J_p .

4.2. Projection onto \mathcal{C}

Step 1 of Algorithm 1 requires to find the orthogonal projection of $a := \begin{pmatrix} m^{(r)} \\ f^{(r)} \end{pmatrix} - \tau \sigma \begin{pmatrix} S_m^T \bar{b}_u^{(r)} \\ S_f^T \bar{b}_v^{(r)} \end{pmatrix}$ onto \mathcal{C} . This means that we have to find a minimizer of $\|Ax - f^-\|_2$ for which $\|a - x\|_2$ attains its smallest value. Substituting $y := a - x$ we are looking for a minimizer y of $\|Ay - Aa + f^-\|_2$ with smallest norm $\|y\|_2$. By [9, Theorem 1.2.10], this minimizer is uniquely determined by $A^\dagger(Aa - f^-)$. Therefore the projection of a onto \mathcal{C} is given by

$$\begin{aligned} \Pi_{\mathcal{C}}(a) &= a - A^\dagger(Aa - f^-) \\ &= a - A^T(AA^T)^\dagger(Aa - f^-). \end{aligned} \quad (16)$$

Note that the projection onto \mathcal{C} coincides with the one onto \mathcal{C}_0 if the given images f_0 and f_1 have the same mass. The Moore-Penrose inverse of the quadratic matrix AA^T is defined as follows: If AA^T has the spectral decomposition

$$AA^T = Q \operatorname{diag}(\lambda_j) Q^T,$$

then it holds

$$(AA^T)^\dagger = Q \operatorname{diag}(\tilde{\lambda}_j) Q^T, \text{ with } \tilde{\lambda}_j := \begin{cases} \frac{1}{\lambda_j} & \text{if } \lambda_j > 0, \\ 0 & \text{otherwise.} \end{cases}$$

The following proposition shows the form of $(AA^T)^\dagger$ in the one-dimensional spatial case. It appears that the projection onto \mathcal{C} amounts to solve a two-dimensional Poisson equation which can be realized depending on the boundary conditions by fast cosine and Fourier transforms.

Proposition 5. *Let C_N , F_N and d^{mirr} , d^{per} be defined as in Appendix A. Then the Moore-Penrose inverse $(AA^T)^\dagger$ in (16) is given by*

$$(AA^T)^\dagger = \begin{cases} (C_P^T \otimes C_{N-1}^T) \operatorname{diag}(\tilde{d}) (C_P \otimes C_{N-1}) & \text{mirror boundary,} \\ (C_P^T \otimes \bar{F}_N) \operatorname{diag}(\tilde{d}) (C_P \otimes F_N) & \text{periodic boundary,} \end{cases}$$

where

$$d := \begin{cases} I_P \otimes N^2 \operatorname{diag}(d_{N-1}^{\text{mirr}}) + P^2 \operatorname{diag}(d_P^{\text{mirr}}) \otimes I_{N-1} & \text{mirror boundary,} \\ I_P \otimes N^2 \operatorname{diag}(d_N^{\text{per}}) + P^2 \operatorname{diag}(d_P^{\text{mirr}}) \otimes I_N & \text{periodic boundary} \end{cases}$$

and $\tilde{d}_j := \frac{1}{d_j}$ if $d_j > 0$ and $d_j = 0$ otherwise.

Proof. By definition of A and using (26), (23), we obtain for periodic boundary conditions

$$\begin{aligned} AA^T &= I_P \otimes (D_N^{\text{per}})^T D_N^{\text{per}} + D_P^T D_P \otimes I_N = I_P \otimes N^2 \Delta_N^{\text{per}} + P^2 \Delta_P^{\text{mirr}} \otimes I_N \\ &= (C_P^T \otimes \bar{F}_N) \text{diag}(I_P \otimes N^2 d_N^{\text{per}} + P^2 d_P^{\text{mirr}} \otimes I_N) (C_P \otimes F_N). \end{aligned}$$

Similarly we get with (26) for mirror boundary conditions

$$\begin{aligned} AA^T &= I_P \otimes D_{N-1}^T D_{N-1} + D_P^T D_P \otimes I_{N-1} = I_P \otimes N^2 \Delta_{N-1}^{\text{mirr}} + P^2 \Delta_P^{\text{mirr}} \otimes I_{N-1} \\ &= (C_P^T \otimes C_{N-1}^T) \text{diag}(I_P \otimes N^2 d_{N-1}^{\text{mirr}} + P^2 d_P^{\text{mirr}} \otimes I_{N-1}) (C_P \otimes C_{N-1}) \end{aligned}$$

which finishes the proof. \square

For the three-dimensional spatial setting we have to solve a four-dimensional Poisson equation. Reordering f and m into large vectors, the matrix form of the operator A is

$$A = \left(I_P \otimes I_3 \otimes I_{N_2} \otimes D_{N_1}^T \mid I_P \otimes I_3 \otimes D_{N_2}^T \otimes I_{N_1} \mid \right. \\ \left. I_P \otimes (D_3^{\text{per}})^T \otimes I_{N_2} \otimes I_{N_1} \mid D_P \otimes I_3 \otimes I_{N_2} \otimes I_{N_1} \right) \quad (17)$$

so that AA^T reads as

$$\begin{aligned} AA^T &= I_P \otimes I_3 \otimes I_{N_2} \otimes D_{N_1}^T D_{N_1} + I_P \otimes I_3 \otimes D_{N_2}^T D_{N_2} \otimes I_{N_1} \\ &\quad + I_P \otimes (D_3^{\text{per}})^T (D_3^{\text{per}}) \otimes I_{N_2} \otimes I_{N_1} + D_P^T D_P \otimes I_3 \otimes I_{N_2} \otimes I_{N_1} \\ &= (C_P^T \otimes \bar{F}_3 \otimes C_{N_2-1}^T \otimes C_{N_1-1}^T) \text{diag}(d) (C_P \otimes F_3 \otimes C_{N_2-1} \otimes C_{N_1-1}), \end{aligned}$$

where

$$\begin{aligned} d &:= I_{3P(N_2-1)} \otimes N_1^2 \text{diag}(d_{N_1-1}^{\text{mirr}}) + I_{3P} \otimes N_2^2 \text{diag}(d_{N_2-1}^{\text{mirr}}) \otimes I_{N_1-1} \\ &\quad + I_P \otimes 3^2 \text{diag}(d_3^{\text{per}}) \otimes I_{(N_2-1)(N_1-1)} + P^2 \text{diag}(d_P^{\text{mirr}}) \otimes I_{3P(N_2-1)(N_1-1)}. \end{aligned}$$

4.3. Schur Complements of $\lambda A^T A + \frac{1}{\tau} I$

To find the minimizer in Step 1 of Algorithm 2 we set the gradient of the functional to zero which results in the solution of the linear system of equations

$$\left(\lambda A^T A + \frac{1}{\tau} I \right) \begin{pmatrix} m \\ f \end{pmatrix} = \lambda A^T f^- + \begin{pmatrix} m^{(r)} \\ f^{(r)} \end{pmatrix} - \tau \sigma \begin{pmatrix} S_m^T \bar{b}_u^{(r)} \\ S_f^T \bar{b}_v^{(r)} \end{pmatrix}.$$

Noting that $\lambda A^T A + \frac{1}{\tau} I$ is a symmetric and positive definite matrix, this linear system can be solved using standard conjugate gradient methods. Alternatively, the next proposition shows how the inverse $(\lambda A^T A + \frac{1}{\tau} I)^{-1}$ can be computed explicitly with the help of the Schur complement and fast sine-, cosine- and Fourier transforms. The proposition refers to the one-dimensional spatial setting but can be generalized to the three-dimensional case in a straightforward way using the appendix.

Proposition 6. *The inverse of the matrix $\lambda A^T A + \frac{1}{\tau} I$ is given by*

$$\begin{pmatrix} I & -X^{-1}Y \\ 0 & I \end{pmatrix} \begin{pmatrix} X^{-1} & 0 \\ 0 & S^{-1} \end{pmatrix} \begin{pmatrix} I & 0 \\ -Y^T X^{-1} & I \end{pmatrix},$$

where

i) *for mirror boundary conditions*

$$\begin{aligned} Y &= D_P^T \otimes D_N, \\ X^{-1} &= I_P \otimes S_{N-1} \text{diag}(\lambda N^2 d_{N-1}^{\text{zero}} + \frac{1}{\tau})^{-1} S_{N-1}, \\ S^{-1} &= (S_{P-1} \otimes C_N^T) \text{diag}(\lambda P^2 d_{P-1}^{\text{zero}} \otimes (1 + \tau \lambda N^2 d_N^{\text{mirr}})^{-1} + \frac{1}{\tau} I) (S_{P-1} \otimes C_N), \end{aligned}$$

ii) *for periodic boundary conditions*

$$\begin{aligned} Y &= D_P^T \otimes D_N^{\text{per}}, \\ X^{-1} &= I_P \otimes F_N \text{diag}(\lambda N^2 d_N^{\text{per}} + \frac{1}{\tau})^{-1} \bar{F}_N, \\ S^{-1} &= (S_{P-1} \otimes F_N) \text{diag}(\lambda P^2 d_{P-1}^{\text{zero}} \otimes (1 + \tau \lambda N^2 d_N^{\text{per}})^{-1} + \frac{1}{\tau} I)^{-1} (S_{P-1} \otimes \bar{F}_N). \end{aligned}$$

Proof. By definition of A we obtain

$$\lambda A^T A + \frac{1}{\tau} I = \begin{pmatrix} \lambda D_m^T D_m + \frac{1}{\tau} I & \lambda D_m^T D_f \\ \lambda D_f^T D_m & \lambda D_f^T D_f + \frac{1}{\tau} I \end{pmatrix} =: \begin{pmatrix} X & Y \\ Y^T & Z \end{pmatrix}$$

so that the inverse can be written by the help of the Schur complement

$$S := Z - Y^T X^{-1} Y$$

as

$$\begin{pmatrix} X & Y \\ Y^T & Z \end{pmatrix}^{-1} = \begin{pmatrix} I & -X^{-1}Y \\ 0 & I \end{pmatrix} \begin{pmatrix} X^{-1} & 0 \\ 0 & S^{-1} \end{pmatrix} \begin{pmatrix} I & 0 \\ -Y^T X^{-1} & I \end{pmatrix}.$$

By (23) and (25) we have with $D \in \{D_N^{\text{per}}, D_N\}$ that

$$\begin{aligned} X^{-1} &= \left(\lambda D_m^T D_m + \frac{1}{\tau} I \right)^{-1} = \left(I_P \otimes \lambda N^2 D D^T + \frac{1}{\tau} I \right)^{-1} \\ &= I_P \otimes (\lambda N^2 D D^T + \frac{1}{\tau} I)^{-1} \\ &= \begin{cases} I_P \otimes S_{N-1} \text{diag}(\lambda N^2 d_{N-1}^{\text{mirr}} + \frac{1}{\tau})^{-1} S_{N-1} & \text{mirror boundary,} \\ I_P \otimes F_N \text{diag}(\lambda N^2 d_N^{\text{per}} + \frac{1}{\tau})^{-1} \bar{F}_N & \text{periodic boundary.} \end{cases} \end{aligned}$$

The Schur complement reads as

$$\begin{aligned} S &= (\lambda D_f^T D_f + \frac{1}{\tau} I) - \lambda^2 D_f^T D_m X^{-1} D_m^T D_f \\ &= (\lambda D_P D_P^T \otimes I_N + \frac{1}{\tau} I) - \lambda^2 (D_P \otimes D^T) \left(I_P \otimes (\lambda N^2 D D^T + \frac{1}{\tau} I)^{-1} \right) (D_P^T \otimes D) \\ &= (\lambda D_P D_P^T \otimes I_N + \frac{1}{\tau} I) - \lambda^2 (D_P D_P^T \otimes D^T (\lambda D D^T + \frac{1}{\tau} I_N)^{-1} D) \\ &= \lambda D_P D_P^T \otimes (I_N - \lambda D^T (\lambda D D^T + \frac{1}{\tau} I_N)^{-1} D) + \frac{1}{\tau} I. \end{aligned}$$

By (22) we have

$$(D_N^{\text{per}})^T = NF_N \text{diag}(-1 + e^{+2\pi i k/n})_k \bar{F}_N$$

and

$$D_N^{\text{per}} = NF_N \text{diag}(-1 + e^{-2\pi i k/n})_k \bar{F}_N$$

so that we obtain for periodic boundary conditions

$$I_N - \lambda(D_N^{\text{per}})^T (\lambda D_N^{\text{per}} (D_N^{\text{per}})^T + \frac{1}{\tau} I_N)^{-1} D_N^{\text{per}} = F_N \text{diag} \left(1 + \tau \frac{1}{\lambda N^2} d_N^{\text{per}}\right)^{-1} \bar{F}_N.$$

Therewith it follows with (25)

$$\begin{aligned} S &= S_{P-1} \text{diag}(\lambda P^2 d_{P-1}^{\text{zero}}) S_{P-1} \otimes F_N \text{diag} \left(1 + \tau \frac{1}{\lambda N^2} d_N^{\text{per}}\right)^{-1} \bar{F}_N + \frac{1}{\tau} I \\ &= (S_{P-1} \otimes F_N) \text{diag} \left(\lambda P^2 d_{P-1}^{\text{zero}} \otimes (1 + \tau \frac{1}{\lambda N^2} d_N^{\text{per}})^{-1} + \frac{1}{\tau}\right) (S_{P-1} \otimes \bar{F}_N) \end{aligned}$$

which yields the assertion for S^{-1} in the periodic case.

For mirror boundary conditions we compute using (24)

$$S = (S_{P-1} \otimes C_N^T) \text{diag} \left(\lambda P^2 d_{P-1}^{\text{zero}} \otimes (1 + \tau \frac{1}{\lambda N^2} d_N^{\text{mirr}})^{-1} + \frac{1}{\tau}\right) (S_{P-1} \otimes C_N)$$

and inverting this matrix finishes the proof. \square

4.4. Proximal Map of J_p

Step 2 of Algorithm 1 consists of an evaluation of the proximal map $\text{prox}_{\frac{1}{\sigma} J_p}$ of J_p . This can be done using the proximal map $\text{prox}_{J_p^*}$ of J_p^* and Moreau's identity $\text{prox}_{\phi}(t) + \text{prox}_{\phi^*}(t) = t$. Therefore, we compute in the following first the dual function J_p^* .

Lemma 7. *For $p \in (1, +\infty)$ and $\frac{1}{p} + \frac{1}{q} = 1$ we have*

$$J_p^*(a, b) = \begin{cases} 0 & \text{if } (a, b) \in \mathcal{K}_p, \\ +\infty & \text{otherwise.} \end{cases}$$

where

$$\mathcal{K}_p := \left\{ (a, b) \in \mathbb{R}^d \times \mathbb{R} : \frac{1}{q} |a|^q + b \leq 0 \right\}.$$

For $p = 2$ this fact can be found in the literature, e.g., in [7]. For convenience we add the proof for arbitrary $p \in [1, +\infty)$.

Proof. By definition, the Fenchel conjugate of J_p is given by

$$J_p^*(a, b) = \sup_{x \in \mathbb{R}^d, y \in \mathbb{R}} \left\{ \langle a, x \rangle + by - J_p(x, y) \right\}.$$

The supremum can only be taken for $y > 0$ and for $(x, y) = (0, 0)$. In the latter case we have $J(a, b) = 0$, so that we can restrict our attention to $y > 0$, that means to

$$J_p^*(a, b) = \sup_{x \in \mathbb{R}^d, y \geq 0} y \left(\left\langle a, \frac{x}{y} \right\rangle + b - \frac{1}{p} \frac{|x|^p}{y^p} \right).$$

We have $J_p^*(a, b) = +\infty$ if $b > 0$, so that it remains to consider $b \leq 0$. Setting the gradient with respect to x and y to zero we obtain

$$\left(a - \frac{|x|^{p-2}x}{y^{p-2}}, b + \frac{1}{q} \frac{|x|^p}{y^p}\right) = (0, 0)$$

so that

$$\frac{|x|^p}{y^p} = q(-b), \quad \frac{x}{y} = a(q(-b))^{-\frac{p-2}{p}}.$$

Using these values in J_p^* we get

$$\begin{aligned} J_p^*(a, b) &= \sup_{y \geq 0} \left\{ y \left(\langle a, a(q(-b))^{-\frac{p-2}{p}} \rangle + b - \frac{1}{p} q(-b) \right) \right\} \\ &= \sup_{y \geq 0} \left\{ y \left(|a|^2 (q(-b))^{-\frac{p-2}{p}} + qb \right) \right\}. \end{aligned}$$

This expression becomes $+\infty$ except for

$$0 \geq |a|^2 (q(-b))^{-\frac{p-2}{p}} + qb,$$

where it is zero. The later inequality is equivalent to

$$\begin{aligned} 0 &\geq |a|^2 (q(-b))^{-\frac{2}{q}} - 1 = \left(|a| (q(-b))^{-\frac{1}{q}} - 1 \right) \left(|a| (q(-b))^{-\frac{1}{q}} + 1 \right), \\ 0 &\geq |a| (q(-b))^{-\frac{1}{q}} - 1, \\ 0 &\geq \frac{1}{q} |a|^q + b. \end{aligned}$$

In summary we see that J_p^* is the indicator function of the set \mathcal{K}_p . □

After this preparation we are now able to compute $\text{prox}_{\frac{1}{\sigma} J_p}$.

Proposition 8. *Let $p \in (1, 2]$ and $\frac{1}{p} + \frac{1}{q} = 1$.*

i) *Then for $x^* \in \mathbb{R}^d$, $y^* \in \mathbb{R}$ and $\sigma > 0$ it holds*

$$\text{prox}_{\frac{1}{\sigma} J_p}(x^*, y^*) = \begin{cases} (0, 0) & \text{if } (\sigma x^*, \sigma y^*) \in \mathcal{K}_p, \\ \left(x^* \frac{h(\hat{z})}{1+h(\hat{z})}, y^* + \frac{1}{\sigma q} \hat{z}^q\right) & \text{otherwise,} \end{cases}$$

where

$$h(z) := (\sigma y^* + \frac{1}{q} z^q) z^{q-2}$$

and $\hat{z} \in \mathbb{R}_{\geq 0}$ is the unique solution of the equation

$$z(1 + h(z)) - \sigma |x^*| = 0 \tag{18}$$

in the interval $[\max(0, z_0)^{\frac{1}{q}}, +\infty)$, where $z_0 := -q\sigma y^*$.

ii) *The Newton method converges for any starting point $z \geq z_0$ quadratically to the largest zero of (18).*

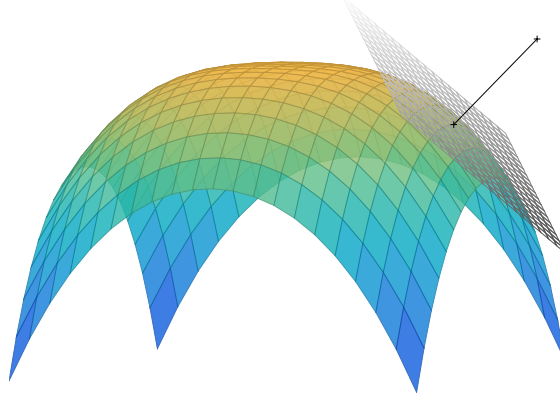


Figure 3: Projection onto the graph of the function $\phi(x) = -\frac{1}{q}|x|^q$ for $q = 3$.

Proof. i) By Moreau's identity it holds $\text{prox}_\phi(t) + \text{prox}_{\phi^*}(t) = t$ and since $(\frac{1}{\sigma}\phi)^*(t) = \frac{1}{\sigma}\phi^*(\sigma t)$ we conclude

$$(\hat{x}, \hat{y}) = \text{prox}_{\frac{1}{\sigma}J_p}(x^*, y^*) = (x^*, y^*) - \frac{1}{\sigma}\text{prox}_{\sigma J_p^*}(\sigma x^*, \sigma y^*), \quad (19)$$

where $\text{prox}_{\frac{1}{\sigma}J_p^*} = \text{prox}_{J_p^*}$ since J_p^* is an indicator function. Note that by definition of J_p we have in particular that $\hat{y} \geq 0$ and $\hat{y} = 0$ only if $|\hat{x}| = 0$. Now, $\text{prox}_{J_p^*}(\sigma x^*, \sigma y^*)$ is the orthogonal projection of $(\sigma x^*, \sigma y^*)$ onto the set \mathcal{K}_p (we could also compute the epigraphical projection of $(\sigma x^*, \sigma y^*)$ onto the epigraph of $\phi(x) = \frac{1}{q}|x|^q$ and reflect y , see also Figure 3).

If $(\sigma x^*, \sigma y^*) \in \mathcal{K}_p$, then $\text{prox}_{J_p^*}(\sigma x^*, \sigma y^*) = (\sigma x^*, \sigma y^*)$ and $(\hat{x}, \hat{y}) = (0, 0)$. So let $(\sigma x^*, \sigma y^*) \notin \mathcal{K}_p$, that means

$$\sigma y^* + \frac{1}{q}|\sigma x^*|^q > 0.$$

The tangent plane of the boundary of \mathcal{K}_p in $(x, y) = (x, -\frac{1}{q}|x|^q)$ is spanned by the vectors $(e_i^\top, -|x|^{q-2}x_i)^\top$, $i = 1, \dots, d$, where $e_i \in \mathbb{R}^d$ denotes the i -th unit vector. Hence, the projection (x, y) is determined by $y = -\frac{1}{q}|x|^q$ and

$$\begin{aligned} 0 &= \left\langle \begin{pmatrix} \sigma x^* \\ \sigma y^* \end{pmatrix} - \begin{pmatrix} x \\ y \end{pmatrix}, \begin{pmatrix} e_i \\ -|x|^{q-2}x_i \end{pmatrix} \right\rangle \\ &= \sigma x_i^* - x_i - (\sigma y^* - y)|x|^{q-2}x_i, \quad i = 1, \dots, d \end{aligned}$$

so that

$$x_i = \frac{\sigma x_i^*}{1 + h(|x|)}, \quad i = 1, \dots, d.$$

Summing over the squares of the last equations gives

$$|x|^2 = |x^*|^2 \frac{\sigma^2}{(1 + h(|x|))^2}.$$

Since a solution has to fulfill

$$\hat{y} = y^* - \frac{1}{\sigma}y = y^* + \frac{1}{q\sigma}|x|^q = \sigma h(|x|)|x|^{2-q} > 0,$$

it remains to search for the solutions with $h(|x|) > 0$. Now, $h(z) > 0$ is fulfilled for $z > 0$ if and only if

$$\sigma y^* + \frac{1}{q}z^q > 0, \tag{20}$$

which is the case if and only if $z > z_0 := \max(0, -q\sigma y^*)^{\frac{1}{q}}$. Then $z := |x|$ has to satisfy the equation

$$z(1 + h(z)) = \sigma|x^*|.$$

The function

$$\varphi(z) := z(1 + h(z)) - \sigma|x^*|$$

has exactly one zero in $[z_0, +\infty)$: By (20) we see that $\varphi(z_0) \leq 0$, but on the other hand we have $\varphi(z) \rightarrow +\infty$ as $z \rightarrow +\infty$, so that φ has at least a zero in $[z_0, +\infty)$. Since $q \geq 2$ for $p \leq 2$ we have for

$$h'(z) = z^{2q-3} + (q-2)(\sigma y^* + \frac{1}{q}z^q)z^{q-3} > 0, \quad z > z_0.$$

Hence h and then also φ is strictly monotone increasing for $z > z_0$. Therefore φ has at most one zero in $[z_0, +\infty)$. Finally, the assertion follows by plugging in (x, y) in (19).

ii) Straightforward computation gives

$$\begin{aligned} h''(z) &= (3q-5)z^{2q-4} + (q-2)(q-3)(\sigma y^* + \frac{1}{q}z^q)z^{q-4}, \\ \varphi'(z) &= 1 + h(z) + zh'(z), \\ \varphi''(z) &= 2h'(z) + zh''(z) \\ &= 3(q-1)z^{2q-3} + (q-1)(q-2)(\sigma y^* + \frac{1}{q}z^q)z^{q-3} > 0, \quad z > z_0. \end{aligned}$$

Since φ is monotone increasing and strictly convex for $z \geq z_0$, the Newton method converges for any starting point $z \geq z_0$ quadratically. \square

5. Numerical Results

In the following we provide several numerical examples. In all cases we used $P = 32$ time steps and 2000 iterations in Algorithm 1 and 2, respectively. The parameters σ and τ were set to $\sigma = 50$ and $\tau = \frac{0.99}{\sigma}$, so that $\sigma\tau < 1$, which guarantees the convergence of the algorithms. Of course, the algorithms do not use tensor products, but relations such as stated in (27) and their higher dimensional versions. If not explicitly stated otherwise, the results are displayed for $p = 2$, in which case the computation of the zeros in (18) slightly simplifies.

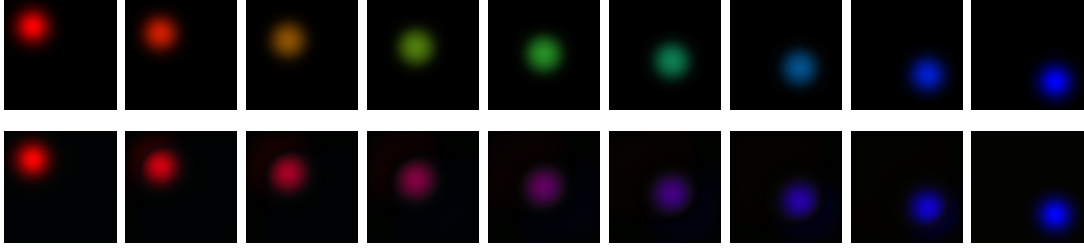


Figure 4: Dynamic optimal transport between a red Gaussian and a blue one with different boundary conditions for the third (color) dimension (top: mirror boundary conditions, bottom: periodic boundary conditions).

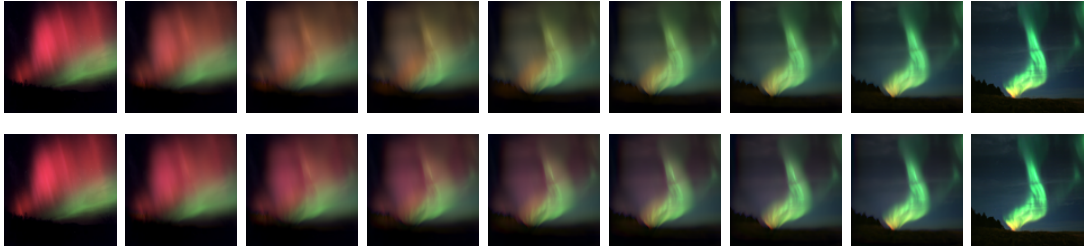


Figure 5: Dynamic color optimal transport between two polar lights (top: mirror boundary conditions, bottom: periodic boundary conditions).

With our first experiment we illustrate the difference between mirror and periodic boundary conditions in the color dimension, where we assume at this point that the initial and the final images have the same mass. The images are displayed at intermediate time-points $t = \frac{i}{8}, i = 0, \dots, 8$. In Figure 4, the transport of a red Gaussian into a blue one is shown, either with mirror or with periodic boundary conditions in the color dimension. Figure 5* depicts the transport between two real images of polar lights. In both cases the use of periodic boundary conditions yields more realistic results.

Further examples of the constraint model (9) for real images are given in Figure 6[†]. In both cases, the initial and final images had approximately the same overall sum of values, so that a rescaling had no significant effect. In the first row of Figure 6, a topographic map of Europe is transported into a satellite image of Europe at night. The second row displays the transport between two images of the Köhlbrandbrücke in Hamburg. In both cases one nicely sees a continuous change of color and shape during the transport. Next we turn to the penalized model (10). Figure 7 shows the influence of the regularization parameter λ when transporting a red Gaussian into a yellow one. Here the initial and the final image have significantly different mass. The images are displayed at intermediate timepoints $t = \frac{i}{8}, i = 0, \dots, 8$. The results change for increasing λ from

*Images from Wikimedia Commons: AGOModra_aurora.jpg by Comenius University under CC BY SA 3.0, Aurora-borealis.andoya.jpg by M. Buschmann under CC BY 3.0.

†Images from Wikimedia Commons: Europe_satellite_orthographic.jpg and Earthlights_2002.jpg by NASA, Köhlbrandbrücke5478.jpg by G. Ries under CC BY SA 2.5, Köhlbrandbrücke.jpg by HafenCity1 under CC BY 3.0.

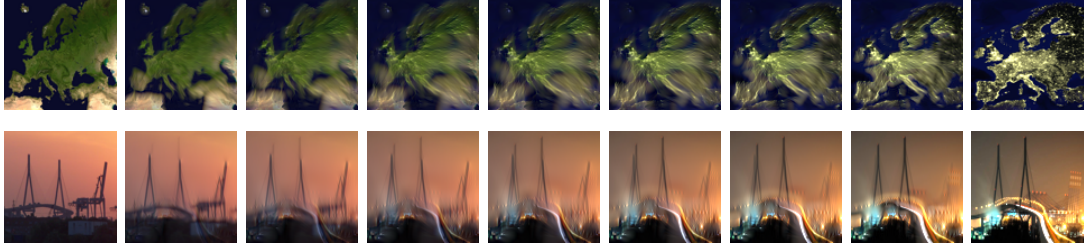


Figure 6: Dynamic color optimal transport between RGB images.

a linear interpolation of the images to a transport of the mass. Further, for large λ the results approach the one obtained with the constrained model (9), which is reasonable. An example for real images is given in Figure 8, where the same observations apply.

Interestingly, we found out that the results obtained with model (9) for different parameters $p \in (1, 2]$ are visually very similar, and any arising differences are of numerical nature. This is in agreement with the theory in the one-dimensional case. For the penalized model (10), however, one can see small differences, compare Figures 9 and 10.

6. Summary and Conclusions

Our contribution can be summarized as follows:

- i) We propose two discrete models for the transport of RGB images which consider color images as three-dimensional objects, where the third direction is reserved for the color information and should be considered to be periodic. We focus on a matrix-vector approach.
- ii) The first model relaxes the continuity constraint so that a transport between images of different mass is possible, while the second model allows even more flexibility by just penalizing the continuity constraint with different regularization parameters.
- iii) An existence proof and a brief discussion on the uniqueness of the minimizer is provided.
- iv) Interestingly, the step in the chosen primal-dual algorithm which takes the continuity constraint into account requires the solution of four-dimensional Poisson equations with simultaneous zero, mirror, and periodic boundary conditions. Here, fast sine-, cosine and Fourier transforms come into the play.
- v) We give a careful analysis of the proximal mapping of J_p , $p \in (1, 2]$. This includes the determination of a starting point for the Newton algorithm to ensure its quadratic convergence and a stable performance of the overall algorithm.
- vi) We show numerous numerical examples.

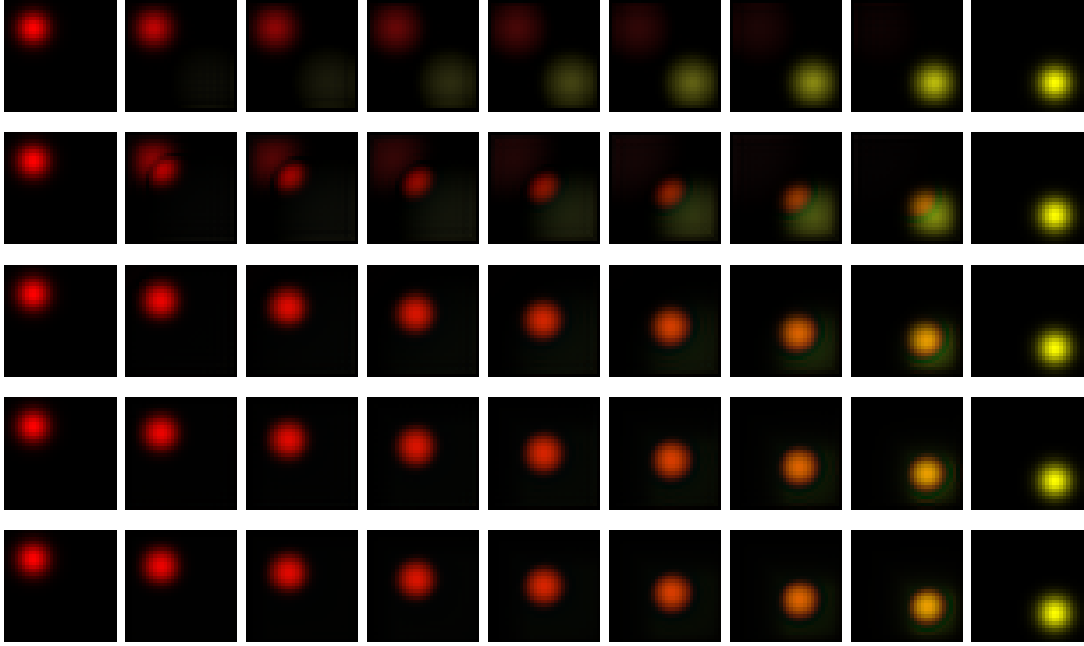


Figure 7: Comparison of penalized and constrained color optimal transport (from top to bottom): penalized optimal transport for different regularization parameters $\lambda \in \{0.1, 1, 10, 100\}$ and constrained optimal transport.



Figure 8: Comparison of penalized and constrained color optimal transport (from top to bottom): penalized optimal transport for different regularization parameters $\lambda \in \{0.1, 0.5, 1, 10\}$ and constrained optimal transport.



Figure 9: Comparison of $p = 2$ (top) and $p = 1.5$ (bottom) for $\lambda = 1$. The images are displayed at intermediate timepoints $t = \frac{i}{4}, i = 0, \dots, 4$.

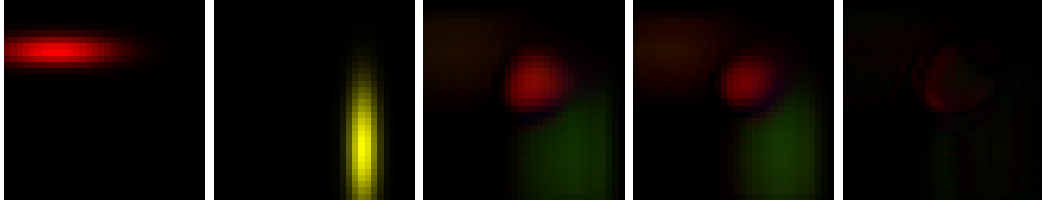


Figure 10: Transport using the penalized model with $\lambda = 1$ for $p = 2$ and $p = 1.5$. From left to right: Initial images f_0, f_1 , result for $p = 2$ and $p = 1.5$ at time $t = 0.5$ and the absolute difference between the two results.

There are several directions for future work. One possibility is to add several additional requirements. For example, the present model has difficulties to transfer sharp contours, which are slightly blurred during the transport. A remedy could be the penalization of a TV-term with respect to f , which results in the functional

$$\operatorname{argmin}_{(m,f) \in \mathcal{C}} \{ \|J_p(S_m m, S_f f + f^+) \|_1 + \gamma \operatorname{TV}(f) \}, \quad \gamma > 0. \quad (21)$$

Figure 11 shows the performance of such a model. Note that in the continuous setting, the consideration of additional properties was addressed with respect to the dissipation in [22].

Acknowledgement: Funding by the DFG within the Research Training Group 1932 is gratefully acknowledged.

A. Diagonalization of Structured Matrices

In the following we collect known facts on the eigenvalue decomposition of various difference matrices. For further information we refer, e.g., to [27, 31]. The following matrices

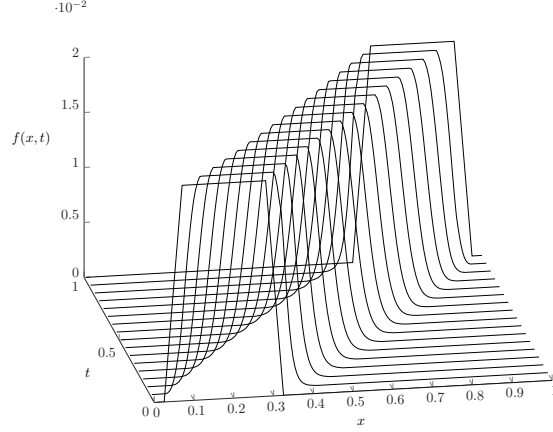


Figure 11: Transport of a one-dimensional signal with sharp edges using the TV penalized functional (21), where $\gamma = 0.03$.

F_n , C_n and S_n are unitary, resp., orthogonal matrices. The Fourier matrix

$$F_n := \sqrt{\frac{1}{n}} \left(e^{\frac{-2\pi i j k}{n}} \right)_{j,k=0}^n$$

diagonalizes circulant matrices, i.e., for $a := (a_j)_{j=0}^{n-1} \in \mathbb{R}^n$ we have

$$\begin{pmatrix} a_0 & a_{n-1} & \dots & a_1 \\ a_1 & a_0 & \dots & a_2 \\ \vdots & & \ddots & \vdots \\ a_{n-1} & a_1 & \dots & a_0 \end{pmatrix} = \bar{F}_n \text{diag}(\sqrt{n} F_n a) F_n = F_n \text{diag}(\sqrt{n} \bar{F}_n a) \bar{F}_n. \quad (22)$$

In particular it holds

$$\begin{aligned} \Delta_n^{\text{per}} &:= \frac{1}{n^2} (D_n^{\text{per}})^T D_n^{\text{per}} = \frac{1}{n^2} D_n^{\text{per}} (D_n^{\text{per}})^T \\ &= \begin{pmatrix} 2 & -1 & & & -1 \\ -1 & 2 & -1 & & \\ & & \ddots & & \\ & & & -1 & 2 & -1 \\ -1 & & & -1 & 2 \end{pmatrix} = \bar{F}_n \text{diag}(d_n^{\text{per}}) F_n \end{aligned} \quad (23)$$

with $d_n^{\text{per}} := (4 \sin^2 \frac{k\pi}{n})_{k=0}^{n-1}$. The operator Δ_n^{per} typically appears when solving the one-dimensional Poisson equation with periodic boundary conditions by finite difference methods.

The DST-I matrix

$$S_{n-1} := \sqrt{\frac{2}{n}} \left(\sin \frac{j k \pi}{n} \right)_{j,k=1}^{n-1},$$

and the DCT-II matrix

$$C_n := \sqrt{\frac{2}{n}} \left(\epsilon_j \cos \frac{j(2k+1)\pi}{2n} \right)_{j,k=0}^{n-1}$$

with $\epsilon_0 := 1/\sqrt{2}$ and $\epsilon_j := 1$, $j = 1, \dots, n-1$ are related by

$$D_n = S_{n-1} \left(0 \mid \text{diag}(\mathbf{d}_{n-1}^{\text{zero}})^{\frac{1}{2}} \right) C_n \quad (24)$$

where $\mathbf{d}_{n-1}^{\text{zero}} := (4 \sin^2 \frac{k\pi}{2n})_{k=1}^{n-1}$. Further they diagonalize sums of certain symmetric Toeplitz and persymmetric Hankel matrices. In particular it holds

$$\begin{aligned} \Delta_{n-1}^{\text{zero}} &:= \frac{1}{n^2} D_n D_n^T \\ &= \begin{pmatrix} 2 & -1 & & & & 0 \\ -1 & 2 & -1 & & & \\ & & \ddots & & & \\ 0 & & & -1 & 2 & -1 \\ & & & -1 & 2 & -1 \end{pmatrix} = S_{n-1} \text{diag}(\mathbf{d}_{n-1}^{\text{zero}}) S_{n-1} \end{aligned} \quad (25)$$

and

$$\begin{aligned} \Delta_n^{\text{mirr}} &:= \frac{1}{n^2} D_n^T D_n \\ &= \begin{pmatrix} 1 & -1 & & & & 0 \\ -1 & 2 & -1 & & & \\ & & \ddots & & & \\ 0 & & & -1 & 2 & -1 \\ & & & -1 & 2 & -1 \end{pmatrix} = C_n^T \text{diag}(\mathbf{d}_n^{\text{mirr}}) C_n \end{aligned} \quad (26)$$

with $\mathbf{d}_n^{\text{mirr}} := \begin{pmatrix} 0 \\ \mathbf{d}_{n-1}^{\text{zero}} \end{pmatrix} = (4 \sin^2 \frac{j\pi}{2n})_{j=0}^{n-1}$. The operators $\Delta_{n-1}^{\text{zero}}$ and Δ_n^{mirr} are related to the Poisson equation with zero boundary conditions and mirror boundary conditions, respectively.

B. Computation with Tensor Products

The tensor product (Kronecker product) of matrices

$$A = \begin{pmatrix} a_{1,1} & \cdots & a_{1,n} \\ \vdots & \cdots & \vdots \\ a_{m,1} & \cdots & a_{m,n} \end{pmatrix} \in \mathbb{C}^{m,n} \quad \text{and} \quad B = \begin{pmatrix} b_{1,1} & \cdots & b_{1,t} \\ \vdots & \cdots & \vdots \\ b_{s,1} & \cdots & b_{s,t} \end{pmatrix} \in \mathbb{C}^{s,t}$$

is defined by the (ms, nt) matrix

$$A \otimes B := \begin{pmatrix} a_{1,1}B & \cdots & a_{1,n}B \\ \vdots & \ddots & \vdots \\ a_{m,1}B & \cdots & a_{m,n}B \end{pmatrix} \in \mathbb{C}^{ms, nt}.$$

The tensor product is associative and distributive with respect to the addition of matrices.

Lemma 9 (Properties of Tensor Products).

i) $(A \otimes B)^T = A^T \otimes B^T$ for $A \in \mathbb{C}^{m,n}$, $B \in \mathbb{C}^{s,t}$.

Let $A, C \in \mathbb{C}^{m,m}$ and $B, D \in \mathbb{C}^{n,n}$. Then the following holds:

ii) $(A \otimes B)(C \otimes D) = AC \otimes BD$ for $A, C \in \mathbb{C}^{m,m}$ and $B, D \in \mathbb{C}^{n,n}$.

iii) If A and B are invertible, then $A \otimes B$ is also invertible and

$$(A \otimes B)^{-1} = A^{-1} \otimes B^{-1}.$$

The tensor product is needed to establish the connection between images and their vectorized versions, i.e., we consider images $F \in \mathbb{R}^{n_1 \times n_2}$ columnwise reshaped as

$$f := \text{vec}(F) \in \mathbb{R}^{n_1 n_2}.$$

Then the following relation holds true:

$$\text{vec}(AFB^T) = (B \otimes A)f. \quad (27)$$

References

- [1] L. Ambrosio, N. Gigli, and G. Savaré. *Gradient Flows in Metric Spaces and in the Space of Probability Measures*. Springer Science & Business Media, 2006.
- [2] S. Angenent, S. Haker, and A. Tannenbaum. Minimizing flows for the Monge-Kantorovich problem. *SIAM Journal of Mathematical Analysis*, 35:61–97, 2003.
- [3] A. Y. Aravkin, J. V. Burke, and M. P. Friedlander. Variational properties of value functions. *SIAM Journal on Optimization*, 23(3):1689–1717, 2013.
- [4] A. Auslender and M. Teboulle. *Asymptotic Cones and Functions in Optimization and Variational Inequalities*. Springer, 2003.
- [5] C. Baiocchi, G. Buttazzo, F. Gastaldi, and F. Tomarelli. General existence theorems for unilateral problems in continuum mechanics. *Archive for Rational Mechanics and Analysis*, 100(2):149–189, 1988.
- [6] J. D. Benamou. A domain decomposition method for the polar factorization of vector-valued mappings. *SIAM Journal of Numerical Analysis*, 32(6):1808–1838, 1995.
- [7] J.-D. Benamou and Y. Brenier. A computational fluid mechanics solution to the Monge-Kantorovich mass transfer problem. *Numerische Mathematik*, 84(3):375–393, 2000.
- [8] M. Bertalmio. *Image Processing for Cinema*. CRC Press, 2014.
- [9] M. Burger, A. Sawatzky, and G. Steidl. First order algorithms in variational image processing. *ArXiv-Preprint 1412.4237*, 2014.

- [10] L. A. Caffarelli. A localization property of viscosity solutions to the monge-ampere equation and their strict convexity. *Annals of Mathematics*, 131(1):129–134, 1990.
- [11] A. Chambolle and T. Pock. A first-order primal-dual algorithm for convex problems with applications to imaging. *Journal of Mathematical Imaging and Vision*, 40(1):120–145, 2011.
- [12] M. J. Cullen. Implicit finite difference methods for modelling discontinuous atmospheric flows. *Journal of Computational Physics*, 81:319–348, 1989.
- [13] M. J. Cullen and R. J. Purser. An extended Lagrangian theory of semigeostrophic frontogenesis. *Journal of Atmospheric Science*, 41:1477–1497, 1989.
- [14] M. Cuturi. Sinkhorn distances: Lighspeed computation of optimal transport. *Advances in Neural Information Processing Systems (NIPS)*, 26:2292–2300, 2013.
- [15] M. Cuturi and A. Coucet. Fast computation of Wasserstein barycenters. *Proceedings of the 31st International Conference on Machine Learning*, 32, 2014.
- [16] B. Dacorogna and P. Maréchal. The role of perspective functions in convexity, polyconvexity, rank-one convexity and separate convexity. *Journal of Convex Analysis*, 15(2):271–284, 2008.
- [17] J.-P. Dedieu. Cônes asymptotes d’un ensemble non convexe. application à l’optimisation. *Compte-rendus de l’Académie des Sciences*, 287:91–103, 1977.
- [18] J. Delon. Midway image equalization. *Journal of Mathematical Imaging and Vision*, 21(2):119–134, 2004.
- [19] J. H. Fitschen, F. Laus, and G. Steidl. Dynamic optimal transport with mixed boundary condition for color image processing. In *International Conference on Sampling Theory and Applications (SampTA) and ArXiv-Preprint 1501.04840*. 2015.
- [20] E. Haber, T. Rehman, and A. Tannenbaum. An efficient numerical method for the solution of the l_2 optimal mass transfer problem. *SIAM Journal of Scientific Computing*, 32(1):197–211, 2010.
- [21] S. A. Kochengin and V. I. Oliker. Determination of reflector surfaces from near-field scattering data. *Inverse Problems*, 13(2):363–373, 1997.
- [22] J. Maas, M. Rumpf, C. Schönlieb, and S. Simon. A generalized model for optimal transport of images including dissipation and density modulation. *ArXiv-Preprint 1504.01988*, 2015.
- [23] N. Papadakis, G. Peyré, and E. Oudet. Optimal transport with proximal splitting. *SIAM Journal on Imaging Sciences*, 7(1):212–238, 2014.
- [24] S. Patankar. *Numerical Heat Transfer and Fluid Flow*. CRC Press, 1980.

- [25] G. Peyré, J. Fadili, and J. Rabin. Wasserstein active contours. In *19th IEEE ICIP*, pages 2541–2544, 2012.
- [26] T. Pock, A. Chambolle, D. Cremers, and H. Bischof. A convex relaxation approach for computing minimal partitions. In *IEEE Conf. Computer Vision and Pattern Recognition*, pages 810–817. 2009.
- [27] D. Potts and G. Steidl. Optimal trigonometric preconditioners for nonsymmetric Toeplitz systems. *Linear Algebra and its Applications*, 281:265–292, 1998.
- [28] J. Rabin, J. Delon, and Y. Gousseau. Transportation distances on the circle. *Journal of Mathematical Imaging and Vision*, 41(1-2):147–167, 2011.
- [29] J. Rabin, G. Peyré, J. Delon, and M. Bernot. Wasserstein barycenter and its application to texture mixing. In *SSVM*, pages 435–446. Springer, 2012.
- [30] R. T. Rockafellar. *Convex Analysis*. Princeton University Press, Princeton, 1970.
- [31] G. Strang and S. MacNamara. Functions of difference matrices are toeplitz plus hankel. *SIAM Review*, 56:525–546, 2014.
- [32] B. Schmitzer and C. Schnörr. A hierarchical approach to optimal transport. In *Scale Space and Variational Methods*, A. Kuijper et al.(Eds.), Springer, Berlin-Heidelberg, pages 452-464. 2013
- [33] T. Teuber, G. Steidl, and R. H. Chan. Minimization and parameter estimation for seminorm regularization models with I-divergence constraints. *Inverse Problems*, 29:1–28, 2013.
- [34] A. Trounev and L. Younes. Metamorphoses through Lie group action. *Foundations of Computational Mathematics*, 5(2):173–198, 2005.
- [35] C. Villani. *Optimal Transport: Old and New*. Springer, Berlin, Heidelberg, 2008.